ELSEVIER

n° 1-4

Chemical Geology 170 (2000) 95–111

CHEMICAL GEOLOGY
INCLUDING
ISOTOPE GEOSCIENCE

www.elsevier.com/locate/chemgeo

Application of in situ-produced cosmogenic ^{10}Be and ^{26}Al to the study of lateritic soil development in tropical forest: theory and examples from Cameroon and Gabon

R. Braucher [a,*], D.L. Bourlès [a], E.T. Brown [b], F. Colin [c], J.-P. Muller [d], J.-J. Braun [e], M. Delaune [d], A. Edou Minko [f], C. Lescouet [g], G.M. Raisbeck [g], F. Yiou [g]

[a] *CEREGE, Université d'Aix Marseille III, Europôle Méditerranéen de l'Arbois, B.P. 80, 13545 Aix en Provence Cedex 4, France*
[b] *Large Lakes Observatory, University of Minnesota, Duluth, MN 55812, USA*
[c] *IRD, UM GECO, CEREGE, Université d'Aix Marseille III, Europôle Méditerranéen de l'Arbois, B.P. 80, 13545 Aix en Provence Cedex 4, France*
[d] *ORSTOM, Laboratoire de Minéralogie-Cristallographie, Universités de Paris 6 et 7, UA CNRS 09, IPGP, Case 115, 4 Place Jussieu, 75252 Paris Cedex 05, France*
[e] *ORSTOM, B.P. 1857, Yaoundé, Cameroon*
[f] *Université de Mavikou, BP 943, Franceville, Gabon*
[g] *Centre de Spectrométrie Nucléaire et de Spectrométrie de Masse, IN2P3-CNRS, Bât. 108, Université Paris-Sud, 91405 Orsay, Cedex France*

Received 25 October 1997; accepted 2 July 1998

Abstract

Depth profiles of in situ-produced cosmogenic nuclides, including ^{10}Be ($T_{1/2} = 1.5 \times 10^6$ years) and ^{26}Al ($T_{1/2}0.73 \times 10^6$ years), in the upper few meters of the Earth's crust may be used to study surficial processes, quantifying denudation and burial rates and elucidating mechanisms involved in landform evolution and soil formations. In this paper, we discuss the fundamentals of the method and apply it to two lateritic sequences located in African tropical forests. © 2000 Elsevier Science B.V. All rights reserved.

Keywords: Cosmogenic nuclides; Lateritic soil development; Tropical forest

1. Introduction

Laterites are widespread surficial formations produced by intense and long-term meteoric weathering of the continental crust. Climatic variations in Africa since the Tertiary have, in addition, induced differentiations in the lateritic texture and topography by weathering and erosional changes. The extent of

* Corresponding author.
E-mail addresses: regis.braucher@libertysurf.fr (R. Braucher), etbrown@d.umn.edu (E.T. Brown), fcolin@cerege.fr (F. Colin), muller@lmcp.jussieu.fr (J.-P. Muller), jean-jacques.braun@lom.camnet.cm (J.-J. Braun).

0009-2541/00/$ - see front matter
PII: S0009-2541(99)00243-0

these physical and chemical changes are, particularly, significant when the climatic conditions occurring during the evolution of the lateritic systems were different from those prevailing during their formation.

In the broad sense (Nahon, 1987; Tardy, 1993), laterites include unconsolidated weathered materials and soils as well as indurated nodules and crusts (ferricretes and bauxite). Although they can exhibit superimposed horizons with different morphologies, laterites are, generally, composed of kaolinite, iron and aluminum oxides, together with residual minerals, such as quartz and muscovite (e.g., Bocquier et al., 1984; Herbillon and Nahon, 1988; Muller et al., 1995). During the last four decades, there have been numerous detailed studies of the mineralogy and the petrology of indurated ferricretes, which are one of the main types of lateritic formation (McFarlane, 1976; Barros-Machados, 1983; Nahon, 1986, 1991; Tardy, 1993; Segalen, 1994). In particular, several authors describe morphological features observed from the base to the top of the weathering profiles and parallel evolutionary sequences of horizons enriched with iron compounds (e.g., Nahon et al., 1977). By contrast, there is much less information on another main type of laterite, the soft clayey, pebbly laterites, which are widespread throughout central Africa and elsewhere and which form on ''half-an-orange''-like hills, under forest cover and in permanently humid and percolating environments (Stoops, 1967; Ojanuga and Lee, 1973; Muller, 1988). One striking characteristic of pebbly laterites is the presence of a ''stone-line'', which may be traced continuously over considerable distances (Vogt, 1966; Lecomte, 1988). Mainly composed of coarse-indurated, ferruginous nodules and quartz gravels, it covers a saprolite and is overlained by a loose clay horizon. Although numerous works have focused on the ''stone-lines'' (see references in Lecomte, 1988), their origin has given rise to much controversy and their formation is still not understood. (1) Did ''stone-lines'' simply differentiate within the soil or were they soil surfaces in the past?; (2) In that latter case, how long did it take to bury them?; (3) What type of processes cause this burial: soil movement, biological activity,...? While autochthonists suggest an ''in situ'' formation of the ''stone-line'' within the lateritic soil, which involves either biological (''bio-pedoturbation'') or chemical processes, according to the authors, allochthonists have related the formation of the ''stone-line'' to some kind of transported overburden.

However, all these works remain mostly qualitative and confined to restricted scale of observation. One of the future challenges in attempting to increase the knowledge of the lateritic systems is to quantify the processes involved both chemically and/or physically in the genesis and the transformation through time of the laterites, in connection with landscape evolution as function of climatic changes. It thus appears necessary to develop new tracers, including pollen (Roche, 1987), phytoliths (Alexandre et al., 1994) gold particles (Colin et al., 1997) and human artifacts (Schwartz, 1996).

In this paper, we quantitatively examine the mechanisms involved in the development of lateritic structures based on measurements of the radioactive cosmogenic ^{10}Be ($T_{1/2}$ = 1.5 Ma) and ^{26}Al ($T_{1/2}$ = 0.72 Ma) concentration produced in the lattice of a primary mineral, the quartz. The study of the evolution of the so-called in situ-produced ^{10}Be and ^{26}Al concentrations along profiles indeed allows us to distinguish between both major dynamic processes affecting surfaces — i.e., erosion and burial, to estimate their rates, and to quantify the extent of bio-pedoturbation. This newly developed technique appears to be a powerful tool to elucidate mechanisms involved in landform evolution and soil formation (Lal, 1987; Bierman, 1994; Brown et al., 1994; Cerling and Craig, 1994). We have applied our method to two examples of representative lateritic systems under rain forest conditions in Cameroon and Gabon.

2. ^{10}Be and ^{26}Al production systematics

Cosmogenic nuclides are produced by nuclear reactions induced, directly or indirectly, by cosmic ray particles (including high energy solar particles) (Raisbeck and Yiou, 1984). In the Earth's atmosphere, ^{10}Be is mainly produced by interactions of the primary cosmic ray particles (α particles and protons) and their secondary particles (neutrons and muons) with atmospheric nuclei of ^{14}N and ^{16}O. Although most of the cosmic ray's energy is dissi-

pated within the atmosphere, reducing cosmic rays intensity by almost 1000 from the top of the atmosphere to sea level, ^{10}Be is also produced in the lithosphere by spallation of ^{16}O, ^{27}Al, ^{28}Si, and ^{56}Fe. In contrast, because the only target for ^{26}Al production in the atmosphere is ^{40}Ar, most ^{26}Al is produced at the Earth's surface, through spallation of ^{27}Al, ^{28}Si, and ^{56}Fe (Lal, 1988).

This paper will focus on using ^{10}Be and ^{26}Al produced in the lattices of rocks exposed to cosmic rays in the upper few meters of the continental crust for studying mechanisms involved in landform evolution and soil formation. The mineral quartz , an ubiquitous material, with a tight crystal structure minimizing diffusion and contamination by meteoric ^{10}Be transported in precipitations appears to be the mineral of choice for such purposes since, in addition, its low content in aluminum— lower than few hundred ppm — facilitates ^{26}Al measurement (Yiou et al., 1984; Lal and Arnold, 1985; Nishiizumi et al., 1986). Furthermore, its ^{16}O and ^{28}Si simple target chemistry is particularly well adapted to the use of in situ-produced ^{10}Be and ^{26}Al for studying surficial processes, the main targets for the ^{10}Be production at the Earth's surface being ^{16}O and ^{28}Si and ^{28}Si for the ^{26}Al production.

Cosmogenic nuclide production rates depend on energy-dependent production cross sections for reactions with the target atoms and on the cosmic ray flux entering the Earth's environment (Lal and Peters, 1967; Raisbeck and Yiou, 1984). The latter parameter is most certainly influenced by the intensity of solar activity (O'Brien, 1979; Raisbeck and Yiou, 1980) but mainly depends on the strength of the Earth's magnetic field (Bard and Broecker, 1992; Robinson et al., 1995) This dependence on field strength, coupled with dissipation of the cosmic radiation within the Earth's atmosphere, are the major reasons for observed latitudinal and altitudinal variability in cosmogenic nuclide production rates. For consistency, production rates are thus commonly given for high latitudes ($> 60°$) and sea level (atmospheric pressure:1033 g cm^{-2}. For ^{10}Be and ^{26}Al, they have been estimated at ~ 6 and ~ 37 atom/g SiO_2/year, respectively (Nishiizumi et al., 1986, 1991a; Lal, 1987; 1988; Brown et al., 1991; Dep, 1995; Clark et al., 1996; Gosse et al., 1996). However, for both cosmogenic nuclides, the production rate for any given altitude and latitude can be estimated fairly accurately using a third degree polynomial deduced from a natural calibration experiment using glacially polished surfaces (Lal, 1991).

Due to the efficient dissipation of their energy through nuclear reactions, the flux of the nuclear active particles in the lithosphere and therefore the cosmogenic nuclide production rates decrease exponentially with the mass of overlying material with a characteristic attenuation length Λ (g cm^{-2}). The evolution of the cosmogenic nuclide production rate ($P_{(x)}$) as a function of depth x — also expressed in g cm^{-2} in order to become independent from the material density — is given by:

$$P(x) = P_0 e^{(-\frac{x}{\Lambda})}, \quad (1)$$

where P_0 is the surface production rate.

Two main types of secondary particles, neutrons and muons, induce in situ-production in the lithosphere. The effective production attenuation lengths of neutrons is short (~ 150 g cm^{-2}) relative to that of muons (~ 1300 g cm^{-2}) (Brown et al., 1995a). This means that although neutron-induced production is dominant in the near-surface (Brown et al., 1995a), below a few meters reactions with muons become dominant.

In addition, Sharma and Middleton (1989) have demonstrated that in most terrestrial materials, and in quartz, in particular, nucleogenic ^{10}Be and ^{26}Al production — i.e., ^{10}Be and ^{26}Al produced by radiation from uranium and thorium and their daughter radionuclides contained within the analyzed samples — is negligible compared to cosmogenic production.

3. ^{10}Be and ^{26}Al concentration evolution

3.1. Eroding surfaces

For a surface undergoing erosion, the abrasion at a rate of ε (g cm^{-2}.year^{-1}) during the time interval dt of a depth interval dx also induces loss in concentration. In that case, the evolution of the ^{10}Be or ^{26}Al concentrations with time and depth are commonly described by the following differential equation:

$$dC = P_0 dt e^{(-\frac{x}{\Lambda})} + \varepsilon dt \frac{dC}{dx} - \lambda C dt. \quad (2)$$

It may be solved to yield:

$$C(x;t) = \frac{P_0 p_n}{\frac{\varepsilon}{\Lambda_n} + \lambda} e^{(-\frac{x}{\Lambda_n})}\left[1 - e^{-t(\frac{\varepsilon}{\Lambda_n} + \lambda)}\right] + \frac{P_0 p_\mu}{\frac{\varepsilon}{\Lambda_\mu} + \lambda} e^{(-\frac{x}{\Lambda_\mu})} \times \left[1 - e^{-t(\frac{\varepsilon}{\Lambda_\mu} + \lambda)}\right] + C_0 e^{(-\lambda t)}, \quad (3)$$

where Λ_n and Λ_μ are the effective attenuation length (g cm^{-2}) for neutrons and muons, respectively, p_n and p_μ the relative contributions of neutrons and muons to the total ^{10}Be production ($p_n + p_\mu = 100\%$), and C_0 the number of atoms present at the initiation of exposure ($p_\mu \sim 1.5\%$ (Braucher et al., 1998)). Since the half-lives of ^{10}Be and ^{26}Al are very short compared to the Earth's age, their primordial component has vanished. In addition, if we assume that the studied rock has undergone a single cosmic ray exposure episode and had no cosmogenic nuclides at the beginning of the present exposure, the initial concentration of cosmogenic nuclides (C_0) equals zero.

As illustrated in Fig. 1, Eq. 3 implies that the cosmogenic nuclide concentrations increase with exposure time until they reach a steady-state balance between production and losses due to erosion and radioactive decay (Lal, 1991). If field observation or other evidence supports the assumption of a simple exposure history and negligible erosion, minimum exposure ages (Fig. 1) can be calculated using:

$$t_{\min} = -\frac{1}{\lambda}\ln\left(1 - \frac{\lambda C_{(0;t)}}{P_0}\right) \quad (4)$$

derived from Eq. 3 for $\varepsilon = 0$.

By contrast, if field evidence indicates an exposure time long enough to reach the steady-state balance concentration, for example, at the surfaces of stable cratons, a maximum erosion rate (Fig. 1) can be computed using:

$$\varepsilon_{\max} = \left(\frac{P_0}{C_{(0;\infty)}} - \lambda\right)\Lambda_n, \quad (5)$$

which is derived from Eq. 3 for $t = \infty$ and makes the reasonable assumption that the surface production is mainly due to neutrons ($p_n \gg p_\mu$).

Theoretical depth distributions of ^{10}Be concentration calculated from Eq. 3 for an infinite exposure time at a range of erosion rates are shown Fig. 2. Surface concentrations are dependent on erosion rates. The form of the exponential decrease in concentration with depth results from the differential attenuation of muons and neutrons in the overlying material. The erosion rate can thus be deduced either from Eq. 5 using the measured ^{10}Be surficial concen-

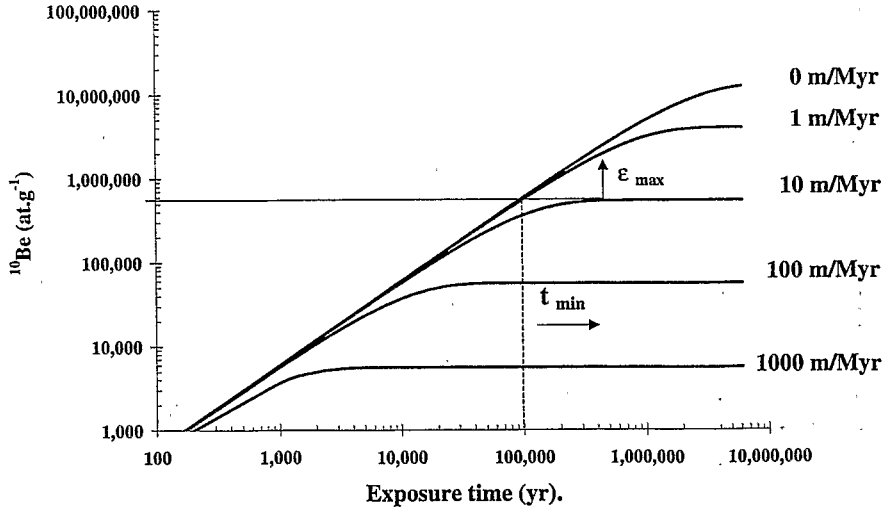

Fig. 1. Theoretical ^{10}Be concentration evolution with exposure time for different erosion rates.

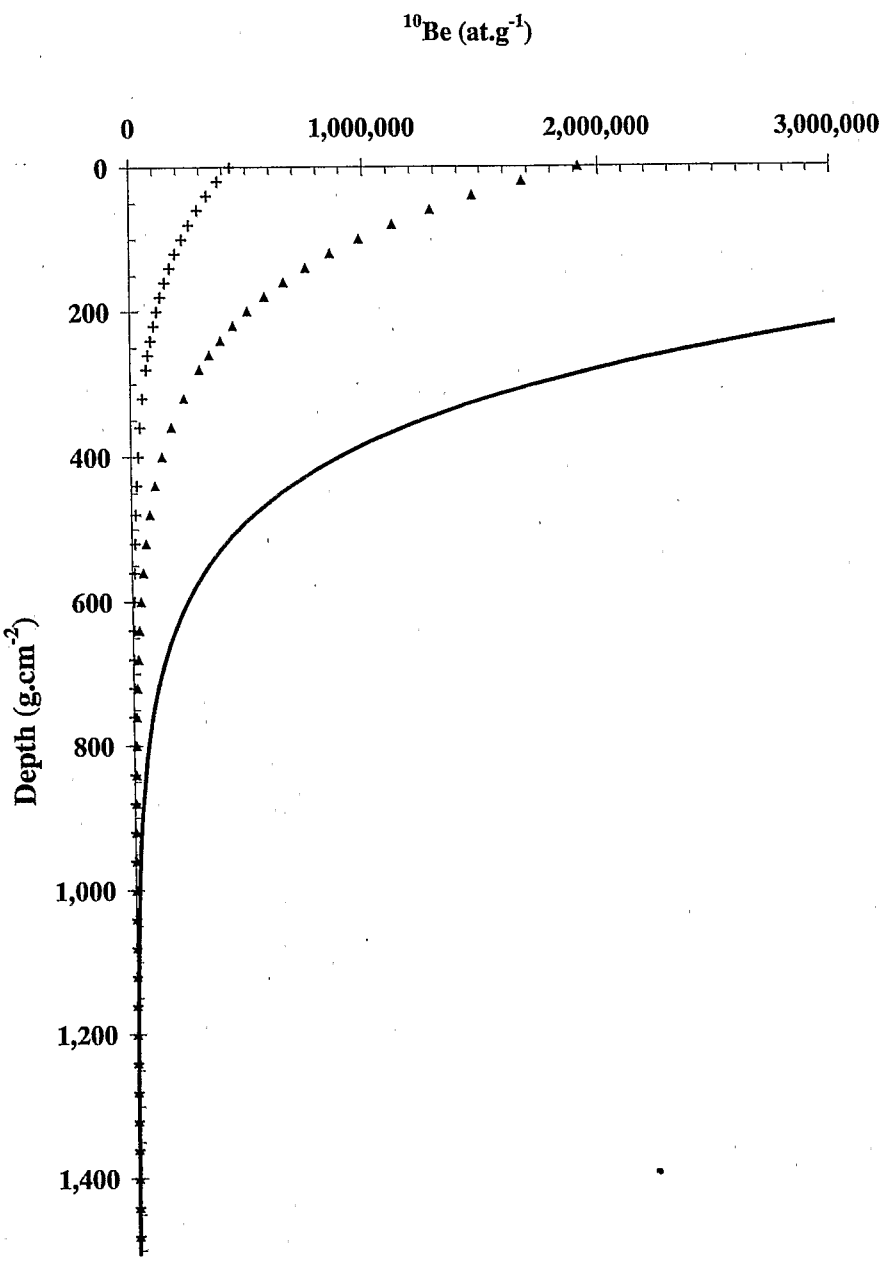

Fig. 2. Theoretical ^{10}Be concentration evolution with depth for three different erosion rates (from left to right 10, 2 and 0 m Ma^{-1}).

tration or from Eq. 3 using the best fit curve technique, the variables being the percentage of muonic production and the erosion rate.

For surfaces undergoing erosion, the maximum possible concentration for a given depth is given by the zero erosion rate curve represented in Fig. 2 by the bold line. The observation of an exponential decrease located in the left part of the zone bounded by the zero erosion rate curve thus characterizes a surface under erosion. This type of distribution implies that the analyzed samples have kept their relative position during the studied exposure episode; it

most likely indicates that the studied surface results from autochthonous in situ chemical weathering.

Along a profile, because of the significantly different attenuation length associated with muons and neutrons, separate determination of ^{10}Be produced by each of the two mechanisms theoretically offers the opportunity to estimate both the exposure age and the erosion rate of surfaces affected by relatively constant denudation rates (Brown et al., 1995a). Because cosmogenic nuclides produced by neutron-induced reactions reach steady state with respect to erosional loss more rapidly than those resulting from muon-induced reactions, ^{10}Be produced at the surface might be used to estimate the erosion rate and that produced at several meters depth to estimate the exposure time.

3.2. Buried surfaces

Environmental changes may induce the burial of surfaces previously under erosion; under these conditions, losses of cosmogenic nuclides due to erosion cease. Cosmogenic nuclide concentrations will thus increase in a rock undergoing burial as long as it remains close enough to the surface so production outweighs radioactive decay (Fig. 3). The ^{10}Be concentration distribution as a function of depth, the product of the time since the initiation of the burial (t_B) and the burial rate (B (g cm^{-2}.year^{-1})), is described by:

$$C(t_B) = \frac{P_0 p_n}{\frac{-B}{\Lambda_n} + \lambda} e^{\left(-\frac{t_B B}{\Lambda_n}\right)} \left[1 - e^{-t_B\left(\frac{-B}{\Lambda_n} + \lambda\right)}\right] + \frac{P_0 p_\mu}{\frac{-B}{\Lambda_\mu} + \lambda} e^{\left(\frac{-t_B B}{\Lambda_\mu}\right)} \left[1 - e^{-t_B\left(\frac{-B}{\Lambda_\mu} + \lambda\right)}\right] + C_0 e^{(-\lambda t_B)}, \quad (6)$$

where C_0 is the concentration at the time of burial.

This implies that the evolution of the ^{10}Be as a function of depth for a profile built from rocks deposited at a constant rate during the burial event (allochthonous processes) is fundamentally different from that for a profile resulting from in-situ weathering mechanisms (autochthonous processes) (Brown et al., 1994). On the other hand, the burial of a previously emplaced profile may result in exponential decreasing ^{10}Be concentrations that are significantly higher for their present depths than those allowed in the zero erosion rate autochthonous scenario (i.e., to the right of the bold line in Fig. 2). The

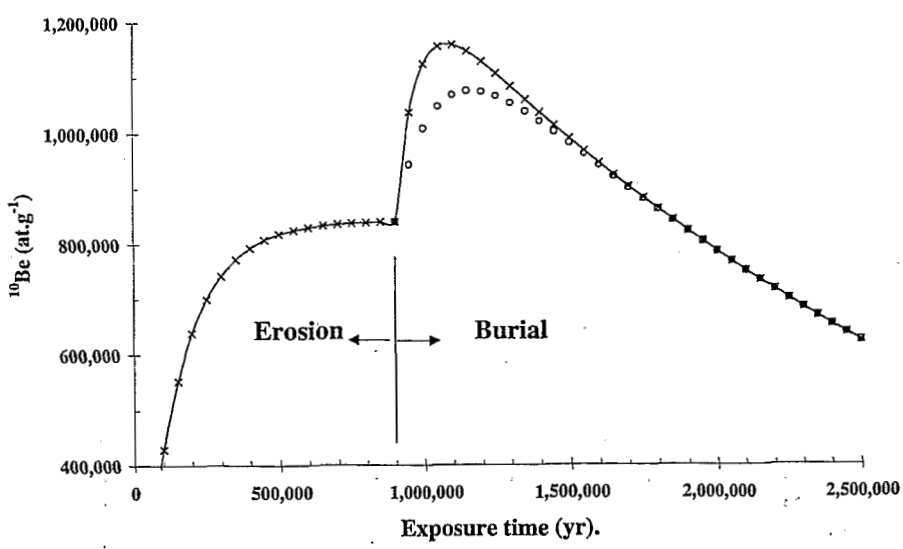

Fig. 3. Theoretical ^{10}Be concentration evolution with exposure time for a surface experiencing, first erosion, then burial. The erosion rate is 5 m Ma^{-1} and, from top to bottom, the burial rates are 5 and 10 m Ma^{-1}.

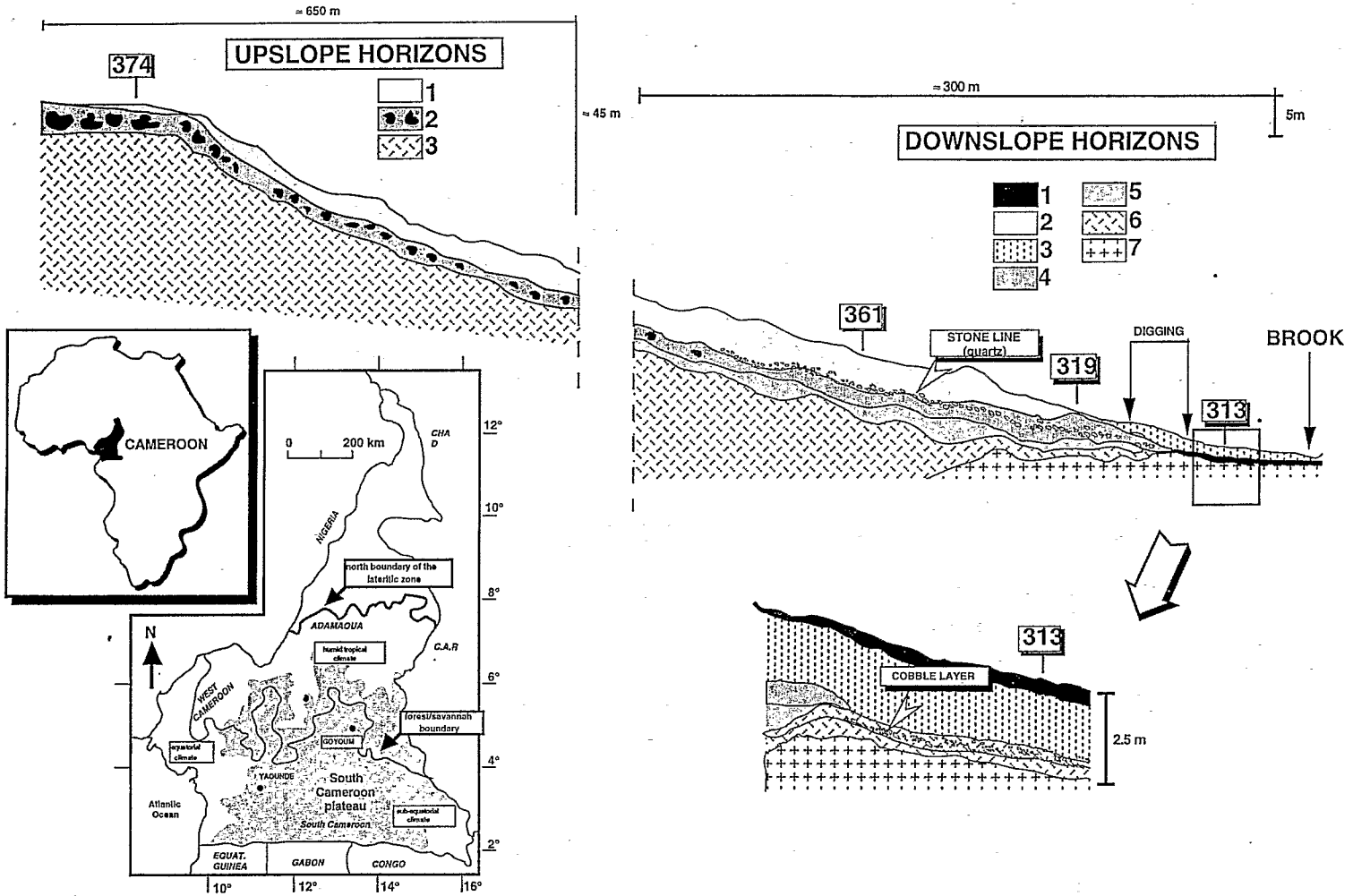

Fig. 4. Sketch map of the Goyoum hill. Downslope horizons: 1 = organic matter accumulation, 2 = soft nodular clayey material, 3 = sandy clayey material, 4 = indurated ferruginous material, 5 = saprolite red material, 6 = yellow saprolitic material, 7 = gneissic parent rock; Upslope horizons: 1 = soft clayey material, 2 = indurated ferruginous material with hardblocks, 3 = saprolite.

study of depth profiles of ^{10}Be thus allows us to distinguish between different surface emplacement scenarios.

3.3. $^{26}Al/^{10}Be$ ratio

When field observations or previous studies suggest a complex history of the investigated site, the ratio ^{26}Al/^{10}Be as a function of the ^{10}Be concentration in the same rock (Lal, 1991; Nishiizumi et al., 1991b) may be used for further evaluation of the mechanisms involved in the evolution of the studied surface. As discussed by Lal (1991), the significantly different radioactive decay constants of both cosmogenic nuclides imply that in the case of any eroding surface the ratio curve vs. nuclide concentration curves can only evolve in a "steady-state erosion island" (Fig. 7). Its upper envelope corresponds to finite exposure times (t) and an erosion rate (ε) equal to zero, i.e.:

$$\frac{C_{26(0;t)}}{C_{10(0;t)}} = \frac{P_{26}\lambda_{10}}{P_{10}\lambda_{26}} \frac{1-e^{-\lambda 10 t}}{1-e^{-\lambda 26 t}}, \quad (7)$$

while its lower envelope corresponds to finite erosion rates and an infinite exposure time, i.e.:

$$\frac{C_{26(\varepsilon;\infty)}}{C_{10(\varepsilon;\infty)}} = \frac{P_{26}}{P_{10}} \frac{\lambda_{10} + \dfrac{\varepsilon}{\Lambda_n}}{\lambda_{26} + \dfrac{\varepsilon}{\Lambda_n}}. \quad (8)$$

When a previously exposed rock is shielded from cosmic radiation due to burial, concentrations of both nuclides decrease through radioactive decay. The rock's cosmogenic nuclide content moves downward and to the left from the "steady-state erosion island". Although there are infinite possible paths (corresponding to complex histories of periodic exposure and burial) to reach values in the lower left portion of the diagram (Lal, 1991), any point will correspond to a minimum burial time which may be calculated as follows: the concentration ratio (R_0) at the initiation of the burial can be expressed as a function of the production rates, the radioactive decay constants and one of the cosmogenic nuclides concentration by applying Eq. 5 to each cosmogenic nuclide, their ε/Λ ratio being equal:

$$R_0 = \frac{C_0^{26}}{C_0^{10}} = \frac{P_{26}}{P_{10} + (\lambda_{26} - \lambda_{10}) C_0^{10}}. \quad (9)$$

The measured C_t^{26}/C_t^{10} ratio (R_t) is then given by:

$$R_t = R_0 e^{-(\lambda_{26} - \lambda_{10})t} = \frac{P_{26} e^{-(\lambda_{26} - \lambda_{10})t}}{P_{10} + (\lambda_{26} - \lambda_{10}) C_0^{10}}. \quad (10)$$

Assuming a burial rate rapid enough to avoid further accumulation after the initiation of the burial, C_0^{10} can be expressed as a function of the measured ^{10}Be concentration as $C_t^{10} e^{\lambda 10 t}$ and Eq. 10 becomes:

$$R_t = \frac{P_{26} e^{(-\lambda_{26} t)}}{P_{10} e^{(-\lambda_{10} t)} + (\lambda_{26} - \lambda_{10}) C_t^{10}}. \quad (11)$$

The minimum burial duration is then obtained by the resolution of Eq. 11. The lower bound should be

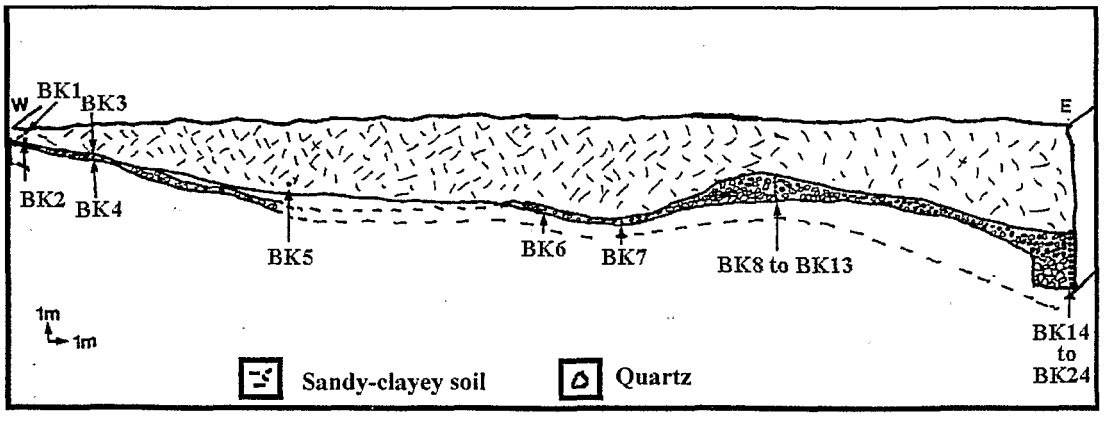

Fig. 5. Schematic cross-section of the Bakoudou soil sequence.

calculated using lower limits for both ^{10}Be production rate and C_t^{26}/C_t^{10} production ratio. For this calculation, we thus decreased ^{10}Be production rates (estimated using the altitude- and latitude-dependent polynomials of Lal, 1991) by their 20% uncertainty and used a minimum value of 5.6 for the C_t^{26}/C_t^{10} production ratio (Nishiizumi et al., 1989).

3.4. Chemical, physical and biological perturbations

As previously discussed by Brown et al. (1995a), in situ-produced cosmogenic ^{10}Be may, in addition, be used to evaluate how depths and relative positions of individual clasts within soil profiles have been affected by chemical weathering, deepening, collapse and bio-pedoturbation.

Under the assumptions that the saprolitic layer is not affected by volume loss so samples maintain their relative positions and that all weathering and volumetric changes occurred after ^{10}Be accumulation, the collapse induced by chemical alteration in the weathered surficial layer can be quantified by comparing actual measured depths with theoretical depths implied by variability of the ^{10}Be concentrations (Eq. 3). Recently, Braucher et al. (1998) validated this approach by demonstrating that the collapse thus calculated is similar to that calculated using zircon as a chemically immobile reference (Colin et al., 1993).

A model of the effects of bio-pedoturbation on cosmogenic nuclide accumulation (Brown et al., 1995b) clearly indicates that this phenomenon increases the time required to reach steady state but has only minor impacts on steady-state concentrations. It implies that the ^{10}Be concentration throughout the surface layer (<2 m) is homogenized to a value similar to that of a surface unaffected by bio-pedoturbation. Below this homogenous layer, and after a transition layer that has been considered as discrete in the discussed model, the ^{10}Be concentrations have a depth variability identical to that of a profile unaffected by bio-pedoturbation (Eq. 3). The determination of the ^{10}Be depth variability along a soil profile may thus permit quantification of the extent of the bio-pedoturbed zone and characterization of the transition layer between the perturbed and unperturbed parts of the profile.

4. Sample preparation

The 0.25–1 mm granulometric quartz fraction sieved from crushed samples has been physically isolated from the other minerals and aggregates by heavy liquids; and chemically purified by selective dissolutions with HCl and H_2SiF_6. To eliminate the potential atmospheric ^{10}Be contamination, the remaining quartz was then cleaned using sequential HF dissolutions (Brown et al., 1991; Kohl and Nishi-

Table 1
^{10}Be results along Goyoum pit profile

Depth (cm)	Mass (g)	Material density (g cm^{-3})	^{10}Be (10^5 atom g^{-1})
Pit 313			
5	24.16	1.37	3.23±0.29
25	27.49	1.37	3.36±0.23
45	26.86	1.60	3.63±0.25
75	23.36	1.67	4.19±0.19
105	23.65	1.67	4.52±0.31
125	24.60	1.79	3.87±0.28
145	24.49	1.79	3.51±0.24
185	25.89	1.5	2.57±0.18
195	23.00	1.48	1.65±0.13
205	22.45	1.56	1.05±0.93
225	21.59	1.56	1.01±0.11
Pit 361			
10	16.95	1.37	6.47±0.70
45	43.35	1.44	6.41±0.90
105	13.83	1.70	7.46±0.83
265	23.69	1.56	5.80±0.40
355	24.31	1.56	4.19±0.44
505	6.25	1.56	4.54±0.58
595	23.07	1.56	3.99±0.33
705	22.47	1.56	2.21±0.21
825	16.21	1.56	0.610±0.10
895	24.15•	1.56	0.64±0.13
985	68.24	1.56	0.21±0.02
Pit 374			
7.5	24.43	1.37	3.82±0.39
25	9.66	1.37	3.93±0.46
35	27.36	1.7	3.43±0.30
55	17.94	1.5	4.91±00.41
95	12.79	1.5	3.61±0.36
215	8.73	1.56	3.22±0.38
425	7.02	1.56	1.01±0.17
525	8.71	1.56	0.62±0.16
895	10.30	1.56	0.44±0.08

izumi, 1992; Cerling and Craig, 1994). The residual cleaned quartz was completely dissolved in HF and spiked with a ^{9}Be carrier (Bourlès, 1988; Brown et al., 1992). Beryllium purified by solvent extractions and alkaline precipitations was prepared for ^{10}Be analyses performed by accelerator mass spectrometry at the Tandétron AMS facility, Gif-sur-Yvette, France (Raisbeck et al., 1987, 1994).

Analytical uncertainties are based on counting statistics (1σ), conservative assumptions of 5% variability in machine response and 50% uncertainty in blank corrections.

5. Applications

To illustrate the principles discussed above, we present the ^{10}Be concentrations measured along profiles from lateritic soils which developed under tropical rain forest in two sites: Goyoum in Cameroon and Bakoudou in Gabon. In addition, ^{26}Al concentrations were measured in "stone-line" samples from Goyoum for better constraint on the evolution of this system.

5.1. Site and sample descriptions

5.1.1. The Goyoum catena

The Goyoum catena, about 600 to 700 m above sea level, which developed on gneissic basement, is located at 5°14′N, 13°18′E in the central-east Cameroon (Fig. 4). This type of "plateau"-like hill develops under forest cover in permanently humid and percolating environments (Muller, 1988).

The catena may be divided in three zones composed of petrographically different materials (Fig. 4).

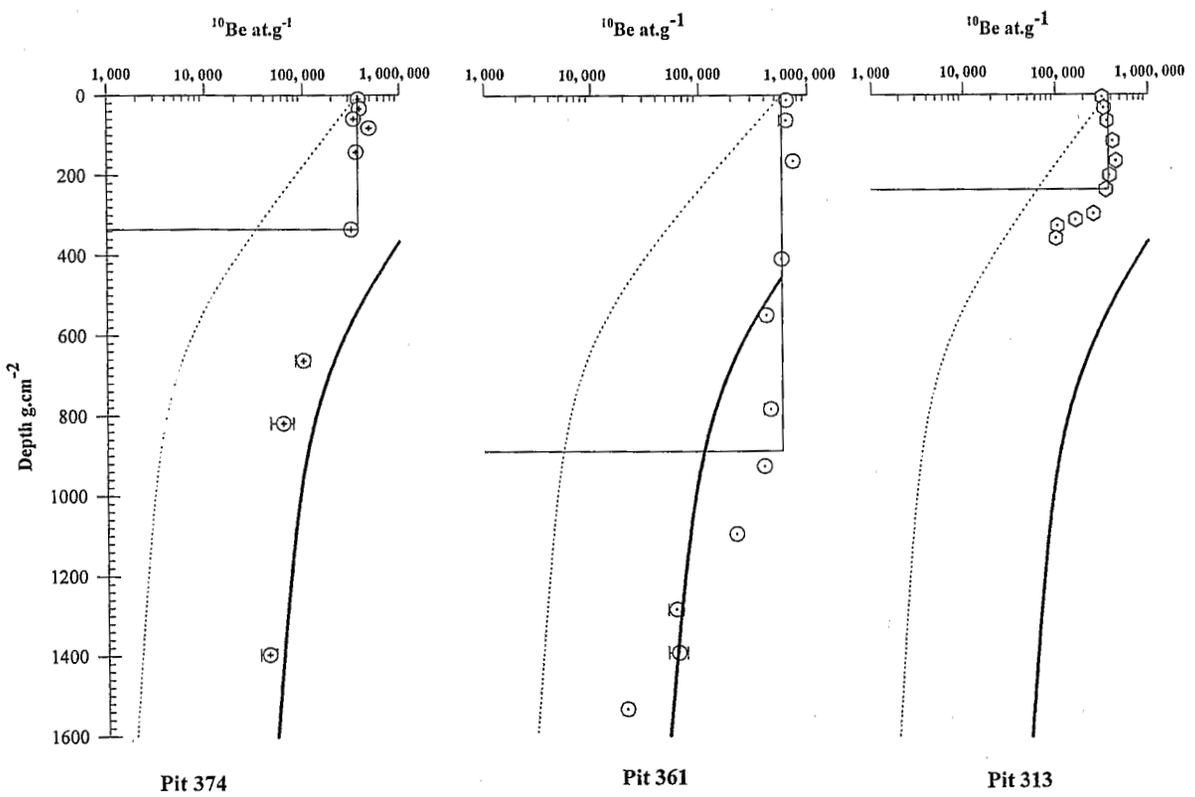

Fig. 6. ^{10}Be concentration evolution as the function of depth along the Goyoum pit profiles. The horizontal line indicates the lowest extent of the bio-pedoturbed zone characterized by the mean ^{10}Be concentration shown by the vertical line. The dotted curve represents the theoretical ^{10}Be concentration exponential decrease using the mean bio-pedoturbed zone ^{10}Be concentration as the surficial value. The bold curve represents the evolution of the ^{10}Be concentration as the function of depth for a zero erosion rate (see text).

Two are located along the slope, the third one being a swampy zone. Three profiles, pits 374, 361 and 313 (see Fig. 4), have been sampled for this study. Profile 374 located on the top plateau belongs to the upslope zone characterized by three superimposed main horizons (Fig. 4): (1) an upper, topsoil horizon of soft clayey material (Bondeulle and Muller, 1988; Muller, 1988; Muller and Bocquier, 1986; Muller and Calas, 1989); (2) an intermediate, nodular horizon composed of indurated, mainly hematitic ferruginous nodules of two types: large nodules with an inherited rock texture and small nodules with a soil texture. All are embedded in soft clayey material; and (3) a lower, soft saprolite with inherited rock texture. Profile 361 is located in the downslope zone, where the lateritic mantle has slightly different characteristics, although three main horizons are again superimposed: (1) a thin yellow, clayey topsoil including ferruginous, hematitic nodules at its bottom; (2) a continuous, goethitic and indurated ferruginous horizon (hardcap), which embeds, at its middle, a line of quartz cobbles; (3) a saprolite with a preserved rock texture containing numerous primary residual minerals at the bottom, where a groundwater table is seasonally present whereas, upwards, it shows more and more red and yellow materials in which the rock texture is no longer preserved. The relative extension of horizons discussed above strongly depends on the topographic position of the profiles: profile 374 shows a diminished topsoil horizon, compared to profile 361 (Fig. 4). It must also be noted that the fresh rock has not been attained in these profiles.

The downslope zone grades to an old alluvial system exhibiting four main horizons from the top to the bottom: (1) an accumulation of organic matter of about 20–40 cm thick; (2) a thick hydromorphic bleached clayey zone, in which rusty spots due to redox change appear upwards; (3) a quartz pebbly layer of presumably alluvial origin, embedded in sandy gneissic matrix; and (4) a thin horizon of weathered bleached gneiss presenting a very sharp contact with the fresh gneiss. The groundwater table is almost outcropping in this zone, where profile 313 has been sampled.

A quartz line is continuously observed from profile 313 to profile 361, although the coarse quartz becomes less and less abundant and less and less rounded from the alluvial system towards the upslope zone. This line crossed laterally the ferruginous horizons, i.e., while it is located near the fresh rock limit in pit 313, it is observed within the ferruginous hardcap in profile 319 and it is indicated by only scarce quartz lying at the upper limit of the nodular horizon in pit 361. Three types of cobbles have been recognized along this quartz line: (1) angular translu-

Table 2
^{10}Be and ^{26}Al results for the Goyoum "stone-line" quartz cobbles

Samples	Depth (cm)	Mass (g)	Material density (g cm^{-3})	^{10}Be (10^5 atom g^{-1})	^{26}Al (10^6 atom g^{-1})	^{26}Al/^{10}Be	Minimum burial time (Ma)
Pit 313							
A.T.[a]	168	30.30	1.50	5.30 ± 0.37	2.54 ± 0.18	4.79 ± 0.48	n.a.[b]
R.M.W. type I[c]	168	18.47	1.50	8.65 ± 0.62	2.81 ± 0.20	3.25 ± 0.33	0.62
R.M.W. type II	168	13.65	1.50	8.39 ± 0.63	2.61 ± 0.19	3.11	0.69
Pit 319							
R.M.W. type I	165	13.08	1.50	4.94 ± 0.70	1.75 ± 0.18	1.81 ± 0.83	1.19
R.M.W. type II	165	6.80	1.50	5.21 ± 0.89	< 3.20	2.07 ± 0.50	1.10
Pit 361							
A.T.	570	24.7	1.56	4.94 ± 0.70	1.75 ± 0.18	2.74 ± 0.44	0.98
R.M.W.	570	4.8063	1.56	5.21 ± 0.89	< 3.20	5.95	n.a.
R.M.W.	570	5.3063	1.56	5.79 ± 0.83	< 1.13	2.87	1.15

[a] Angular translucent.
[b] Non applicable.
[c] Rounded milk white (type I: microcrystalline structure type II: millimetric size crystalline structure).

cent (A.T.); (2) rounded milky quartz with a microcrystalline structure (R.M.W., Type I); (3) rounded milky quartz with a millimetric crystalline structure (R.M.W., Type II). No coarse quartz has been observed in pit 374.

5.1.2. The Bakoudou sequence

The Bakoudou sequence, about 550 and 600 m above sea level, is located at 2°S; 13°21 E in the south-east Gabon at the limit of the equatorial forest and savanna (Fig. 5). The regional landscape is mainly composed of ''half-an-orange''-like hills that are commonly considered as representing the emerged part of the chemically weathered underlying saprolite.

Samples have been collected from a trench at the base of a rounded hill:

quartz cobbles BK1 to BK13 from a quartz-rich ''stone-line'' in the median layer recovered by a surficial sandy clayey layer
quartz cobbles BK14 to BK24 from a vein within the saprolite at the base of the weathering mantle.

5.2. Results and discussion

5.2.1. The Goyoum catena

The ^{10}Be concentrations measured along profiles from several pits from the bottom to the top of the hill show the same type of distribution: a quasi-constant concentration in the uppermost horizon followed by an exponential decrease in the saprolitic layer (Table 1 and Fig. 6). In pits 361 and 374, the nodular horizon level may be considered as a transition zone with ^{10}Be concentrations rapidly decreasing from their topsoil horizon value to the value at the top of the saprolitic unit.

In all studied pits, the ^{10}Be concentrations measured in the uppermost horizon are not significantly different along a given profile. This characterizes a bio-pedoturbed zone as modeled by Brown et al. (1995b). The study of the distribution of the in situ-produced ^{10}Be concentration in quartz mineral from surficial horizon profiles then allows us to quantify unambiguously the extent of the homogenized bio-pedoturbed zone: 2.40, 1.65 and 5.70 m at pits 374, 313 and 361, respectively. It is interesting

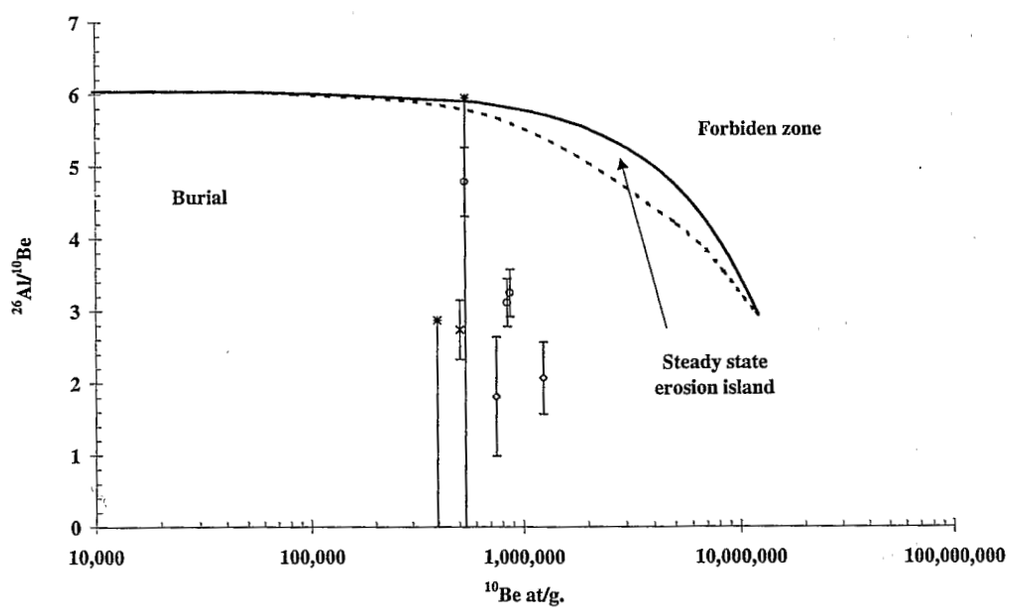

Fig. 7. ^{26}Al/^{10}Be ratio vs. ^{10}Be concentration for the Goyoum ''stone-line'' quartz cobbles. The bold curve corresponds to finite exposure times (t) and an erosion rate (ε) equal to zero and the dashed curve corresponds to finite erosion rates and an infinite exposure time. These curves have been calculated using lower limits for the ^{10}Be production rate and ^{26}Al/^{10}Be production ratio (see text). Open circles correspond to pit 313 experimental data; open diamonds correspond to pit 319 experimental data and crosses correspond to pit 361 experimental data.

to note that the base of the bio-pedoturbed zone corresponds to the interface either with the nodular horizon in pits 361 and 374 or with the quartz line in pit 313. The quartz pebbly layer tightly sampled within pit 313 appears to be a transition zone, where the ^{10}Be concentration dramatically decreases from its homogenized uppermost horizons value to that of the underlying unperturbed saprolite. Unfortunately, because of the outcropping groundwater table, the 313 pit's saprolite has only been sampled at its interface with the quartz pebbly layer. In the contrary, while the lack of quartz minerals prevents us to study the transition zone in pit 374, the saprolitic material has been satisfactorily sampled. The exponential ^{10}Be concentration decrease as a function of depth in the saprolite observed in this top plateau pit is in a good agreement with that implied by a zero erosion model considering that 1.5% of the total ^{10}Be production is induced by muons (Braucher et al., 1998).

The sampling at pit 361 also permits examination of the in situ-produced ^{10}Be concentration variation as a function of depth within the saprolitic layer. Although, as expected, an exponential decrease is observed, measured ^{10}Be concentrations significantly higher than that allowed in the zero erosion rate autochthonous scenario are evidenced (Fig. 6). As discussed above, this suggests that the Goyoum sequence may have experienced burial. The apparent attenuation length of 194 g cm^{-2} calculated from pit 361 data is considerably lower than what would be anticipated for material exposed at depths great enough for muon-induced reactions to be the dominant production mechanism (Fig. 6). This indicates that material in the bio-pedoturbed surface layer was deposited over a previously exposed surface or that material below bio-pedoturbed layer had been mixed with surficial material in past. In order for the evolution of the Goyoum lateritic soil sequence to be precise, both ^{10}Be and ^{26}Al cosmonuclide concentrations have been measured in quartz pebbles from the ''stone-line'' present through the nodular horizon. The previously defined types of ''stone-line'' quartz pebbles were analyzed in both pits 313 and 361. Since Type I and Type II concentrations appear to be not significantly different for these two pits, both types were mixed before measurements for intermediate pit 319 (R.M.W., Table 2). Given their present depths, ''stone-line'' pebbles from pit 361 have ^{10}Be concentrations that are significantly higher than those allowed in the zero erosion rate autochthonous scenario, allowing us to conclude that in the past they were closer to surface. In contrast, ''stone-line'' quartz pebble ^{10}Be concentrations by themselves are not conclusive for pit 313 and pit 319. Examining ^{26}Al in conjunction with ^{10}Be provides more detailed information on the burial history of these samples. In ^{26}Al/^{10}Be–^{10}Be space, all ''stone-line'' quartz pebbles fall to the left side of the ''steady-state erosion island'' (Fig. 7). This confirms the occurrence of burial at Goyoum. The minimum burial times estimated, when possible, for each cobble type in each pit range from ~0.7 Ma for the lowest value (pit 313) to ~1.2 Ma for the highest value (pit 319) (Table 2), corresponding to burial rates on the order of a few meters per million years.

5.2.2. *The Bakoudou sequence*

Most of the ^{10}Be concentrations measured in quartz cobbles from this site (Table 3 and Fig. 8) are

Table 3
Bakoudou's sequence ^{10}Be results

Samples	Depth (cm)	Mass (g)	Material density (g cm^{-3})	^{10}Be (10^5 atom g^{-1})
BK-1	50	29.54	1.5	2.74±0.30
BK-2	60	26.71	1.8	2.14±0.19
BK-3	150	29.58	1.5	1.40±0.15
BK-4	170	26.66	1.8	1.16±0.13
BK-5	330	28.79	1.5	9.73±0.64
BK-6	480	29.69	1.5	15.70±0.96
BK-7	530	31.06	1.5	8.50±0.54
BK-8	300	26.76	1.5	10.20±0.61
BK-9	320	33.41	1.8	1.66±0.42
BK-10	350	26.34	1.8	2.78±0.21
BK-12	400	27.43	1.8	0.98±0.12
BK-13	430	26.39	1.8	0.93±0.01
BK-14	580	41.34	1.5	7.39±0.41
BK-15	600	43.96	1.8	3.68±0.23
BK-16	630	32.18	2.6	2.53±0.19
BK-17	670	36.62	2.6	1.63±0.15
BK-18	690	39.66	2.6	1.74±0.16
BK-19	730	41.58	2.6	1.37±0.11
BK-20	750	31.36	2.6	9.42E±0.10
BK-21	775	29.02	2.6	1.13±0.11
BK-22	800	33.53	2.6	1.09±0.11
BK-23	820	26.08	2.6	1.39±0.15
BK-24	850	27.07	2.6	0.78±0.08

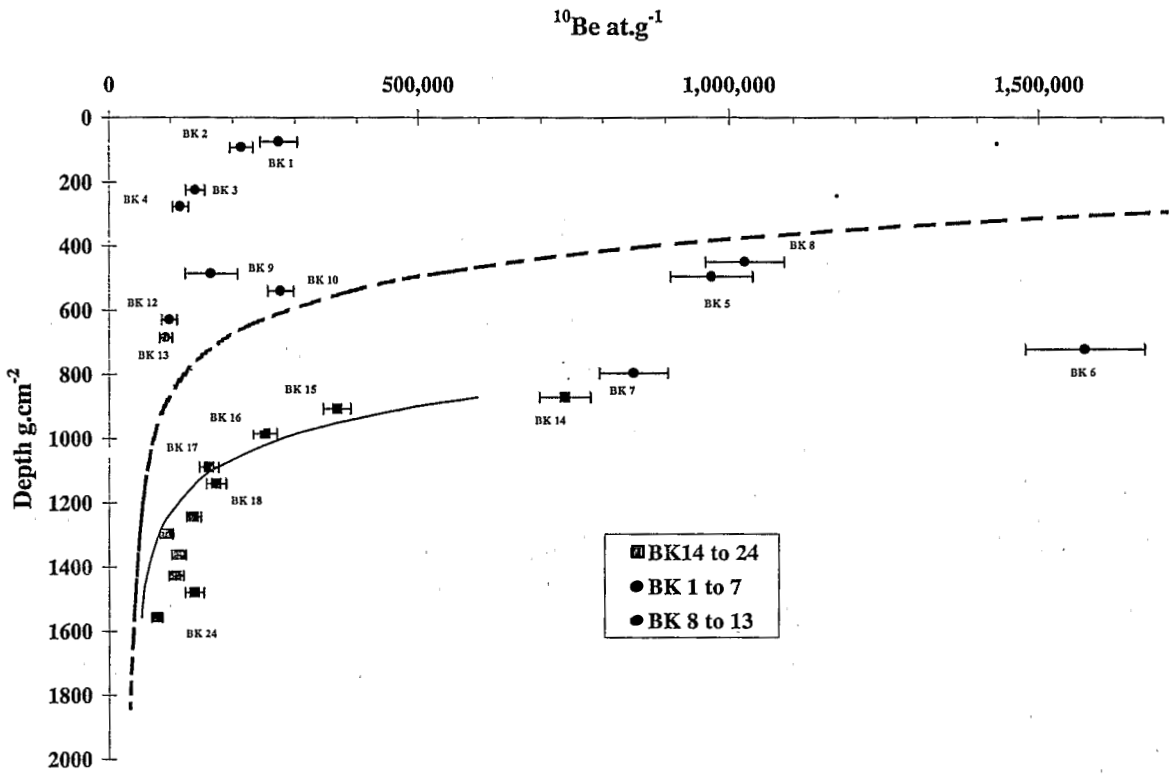

Fig. 8. ^{10}Be concentration evolution as a function of depth for Bakoudou samples. The dashed line represents the evolution of the ^{10}Be concentration as the function of depth for a zero erosion rate. The bold curve corresponds to the best fit curve to the quartz vein experimental points using Eq. 6. The best fit yields to: (1) a "paleo erosion" rate of 2.0 ± 0.3 m Ma^{-1} and (2) a burial rate of 45 ± 10 m Ma^{-1} with a muonic production percentage to the total ^{10}Be production rate fixed at 1.5%.

higher than those allowed in the zero erosion rate autochthonous scenario, most likely indicating the occurrence of a burial event.

Samples from the lower part of the quartz vein penetrating the saprolite (BK24 to BK15) show an exponential decrease with an attenuation length of 155 g cm^{-2}, which not only implies that they have maintained their relative positions for most of their exposure history (Collinet, 1969) but also that the vein spent most of its history nearer to the surface. If significant, the flattening of the exponential curve induced by the uppermost sample of the vein (BK14) may correspond to a chemical weathering induced collapse (Braucher et al., 1998).

The ^{10}Be concentrations of samples BK7 and BK6 located in the "stone-line", which develops at the saprolite–sandy clayey layer interface, appear to be in line with an extrapolation of the exponential curve described above. This indicates that they have remained in the same relative positions with respect to the quartz vein.

Samples BK8 to BK13 belong to an accumulation of quartz cobbles at the saprolite–sandy clayey layer interface. Their ^{10}Be concentrations generally fall within the zero erosion envelope. Even if their ^{10}Be concentrations do not allow us to link them to the samples previously discussed, field observations strongly suggest that they belong to the paleo-erosional surface and have most likely experienced burial as the quartz vein. The burial scenario is also in agreement with the ^{10}Be concentration of the BK5 sample from the bottom of the sandy clayey layer.

By contrast, the much lower ^{10}Be concentrations of samples BK1 to BK4 alone do not allow us to firmly associate them to the same emplacement mechanism.

This large dataset was used to quantify the parameters characterizing the evolution of the Bakoudou

sequence. The proposed model is based on the samples from the quartz vein, i.e., BK24 to BK14. Its aim is to estimate the burial rate affecting the site. In order to reach that goal, the initial ^{10}Be concentration has first to be quantified (see Eq. 6). Considering that the observed exponential decrease is inherited from the exposure history before burial, a surficial profile with theoretical sampling points having the same relative depth positions generated using Eq. 3 replaces the C_0 term of Eq. 6. The tunable parameters being thus: (1) the erosion rate prior burial; (2) the burial rate, the best fit to the experimental values (Fig. 8) yield to: (1) a ''paleo-erosion'' rate of 2.0 ± 0.3 m Ma^{-1}; (2) a burial rate of 45 ± 10 m Ma^{-1} with a muonic production percentage to the total ^{10}Be production rate fixed at 1.5% (Brown et al., 1995a; Braucher et al., 1998). While, as indicated by the uncertainties associated with our estimates, this model appears to be relatively sensitive to variations of the ''paleo-erosion'' rate, it is less sensitive to burial rate variations. However, such high burial rates are not uncommon in tropical humid zones (Tricart, 1976); soil may become saturated and mechanically unstable during heavy and prolonged rains. This, phenomenon is of course accentuated by the relief and deforestation. Landslides must therefore, be taken into account while considering the processes which may lead locally to the emplacement of ''stone-lines''.

6. Conclusion

In situ-produced cosmogenic nuclides ^{10}Be ($T_{1/2}$ = 1.5 Ma) and ^{26}Al ($T_{1/2}$ = 0.72 Ma) appear to be powerful tools for quantitative study of the mechanisms involved in the evolution of the Earth's surface. In particular, the study of the variations of their concentrations along profiles allows us to quantitatively establish the various processes involved in the development of lateritic surfaces today localized in tropical forest.

The extent of bio-pedoturbation in the upper soil layers has been clearly demonstrated through the measurements of ^{10}Be concentrations in material from several soil pits at the Goyoum hill (Cameroon). In addition, the ^{10}Be concentrations measured in the saprolite of this site indicate the occurrence of burial during the development of the studied sequence. This is confirmed by examination of the ^{26}Al/^{10}Be ratio as a function of the ^{10}Be concentration measured in quartz cobbles from the ''stone-line'' travelling through the nodular layer. Moreover, the combined used of both cosmogenic nuclides permits to calculate the ''stone-line'' minimum burial time.

In Gabon, the ^{10}Be concentration measurements of many samples along a quartz vein and along its apparently connected ''stone-line'' allow us to develop a quantitative model describing the processes involved in the evolution of the Bakoudou hill.

Acknowledgements

We thank J. Lestringuez and D. Deboffle for their continuing expertise in AMS measurements. Fieldwork was facilitated by the logistic support of ORSTOM Centers (Yaoundé and Brazzaville). This work was supported by INSU-CNRS through the DBT Program Thème 1: ''Fleuves et érosion'' by INSU-CNRS and ORSTOM through the PEGI Program. Tandétron operation is supported by the CNRS, CEA and IN2P3.

References

Alexandre, A., Colin, F., Meunier, J.D., 1994. Les phytolithes, indicateurs du cycle biogéochimique du silicium en forêt équatoriale. C. R. Acad. Sci. Paris 319 II (4), 453–458.

Bard, E., Broecker, W.S., 1992. The last deglaciation: absolute and radiocarbon chronologies. Series I: Global Environmental Change Vol. 2 Springer-Verlag, Berlin.

Barros-Machados, A., 1983. The contribution of termites to the formation of laterites. In: Carvalho, A.J.M.e.A. (Ed.), Ils. Intern. Seminar on Laterisation Processes. Sao Paulo, Brazil, pp. 262–270.

Bierman, P.R., 1994. Using in situ produced cosmogenic isotopes to estimate rates of landscapes evolution: a review from the geomorphic perspective. J. Geophys. Res. 99 (B7), 13885–13896.

Bocquier G., Muller J.P., Boulangé B., 1984. Les latérites., Livre jubilaire du cinquantenaire de l' Association Française pour l'étude du Sol. C.N.R.S, I.N.R.A, O.R.S.T.O.M, M.I.D.I.S.T., pp. 123-138.

Bondeulle, G., Muller, J.P., 1988. Structural characteristics of hematite and goethite and their relationships with kaolinite in a laterite from Cameroon. A TEM study. Bull. Mineral. 111, 149–166.

Bourlès D.L., 1988. Etude de la géochimie de l'isotope

cosmogénique ^{10}Be et de son isotope stable ^{9}Be en milieu océanique. Application a la datation des sédiments marins. PhD Thesis, Paris-sud Centre d'Orsay.

Braucher, R., Bourlès, D.L., Brown, E.T., Colin, F., Muller, J.P., Braun, J.J., Delaune, M., Lescouet, C., Raisbeck, G.M., Yiou, F., 1998. Examination of lateritic system and rain forest soil development using in situ-produced ^{10}Be. Geochim. Cosmochim. Acta 69-9, 1501–1509.

Brown, E.T., Bourlès, D.L., Colin, F., Yiou, F., Desgarceaux, S., 1995a. Evidence for muon-induced production of ^{10}Be in near-surface rocks from the Congo. Geophys. Res. Lett. 22 (6), 703–706.

Brown, E.T., Bourlès, D.L., Colin, F., Sanfo, Z., Raisbeck, G.M., Yiou, F., 1991. Examination of surface exposure ages of Antartic moraines using in situ produced ^{10}Be and ^{26}Al. Geochim. Cosmochim. Acta 55, 2269–2283.

Brown, E.T., Bourlès, D.L., Colin, F., Sanfo, Z., Raisbeck, G.M., Yiou, F., 1994. The development of iron crust lateritic systems in Burkina Faso, West Africa examined with in-situ-produced cosmogenic nuclides. Earth Planet. Sci. Lett. 124, 19–33.

Brown, E.T., Brook, E.J., Raisbeck, G.M., Yiou, F., Kurz, M.D., 1992. Effective attenuation lengths of cosmic rays producing ^{10}Be and ^{26}Al in quartz: implications for exposures ages dating. Geophys. Res. Lett. 19 (4), 369–372.

Brown, E.T., Stallard, R.F., Larsen, M.C., Raisbeck, G.M., Yiou, F., 1995b. Denudation rates determined from the accumulation of in situ-produced ^{10}Be in Luquillo experimental Forest, Puerto Rico. Earth Planet. Sci. Lett. 129, 193–202.

Cerling, T.E., Craig, H., 1994. Geomorphology and in situ cosmogenic isotopes. Annu. Rev. Planet. Sci. 22, 273–317.

Clark, D.H., Bierman, P.R., Larsen, P., 1996. Improving in situ cosmogenic chronometers. Quat. Res. 44, 366–376.

Colin, F., Alarcon, C., Vieillard, P., 1993. Zircon: an immobile index in soils? Chem. Geol. 107, 273–276.

Colin, F., Sanfo, Z., Brown, E.T., 1997. Gold: a tracer of the dynamics of tropical soils. Geology 25 (1), 81–84.

Collinet, J., 1969. Contribution à l'étude des "stone-lines" dans la région du Moyen-Ogooé (gabon). cahiers O R.S.T.O.M. sér. Pedologie VII (1), 3–42.

Dep, L., 1995. Cosmogenic radionuclide production in terrestrial rocks: accelerator mass spectrometry measurements and Monte carlo simulations. PhD Thesis, Purdue, Purdue, 155 pp.

Gosse, J.C., Reedy, R.C., Harrington, C.D., Poths, J., 1996. Overview of the workshop on the secular variations in production rates of cosmogenic nuclides on earth. Radiocarbon 38 (1), 135–173.

Herbillon, A.J., Nahon, D., 1988. Laterites and lateritization processes. In: Stucki, B.A.G.a.U.S.W. (Ed.), Iron in Soils and Clay Minerals. Reidel, Dordrecht, pp. 779–796.

Kohl, C.P., Nishiizumi, K., 1992. Chemical isolation of quartz for measurements of in situ produced cosmogenic nuclides. Geochim. Cosmochim. Acta 56, 3583–3587.

Lal, D., 1987. Cosmogenic nuclides produced in situ in terrestrial solids. Nucl. Instrum. Methods Phys. Res., Sect. B 29, 238–245.

Lal, D., 1988. In situ produced cosmogenic isotopes in terrestrial rocks. Annu. Rev. Earth Planet. Sci. 16, 355–388.

Lal, D., 1991. Cosmic ray labeling of erosion surfaces: in situ nuclide production rates and erosion models. Earth Planet. Sci. Lett. 104, 424–439.

Lal, D., Arnold, J.R., 1985. Tracing quartz through environment. Proc. Indian Acad. Sci. (Earth Planet. Sci.) 94 (1), 1–5.

Lal, D., Peters, B., 1967. Cosmic ray produced radioactivity on the earth. In: Flugge, S. (Ed.), Handbook of Physics. Springer-Verlag, Berlin, pp. 551–612.

Lecomte, P., 1988. Stone line profiles: importance in geochemical exploration. J. Geochim. Explor. 30, 35–61.

McFarlane, M.J., 1976. Laterites. Laterite and Landscape. Academic Press, London, p. 151.

Muller, J.P., 1988. Analyse pétrologique d'une formation latéritique meuble du Cameroun. Essai de traçage d'une différenciation supergène par les paragénèses minérales secondaires 50, 664, Orstom, Paris.

Muller, J.-P., Bocquier, G., 1986. Dissolution of kaolinites and accumulation of iron oxides in lateritic-ferruginous nodules. Mineralogical and microstructural transformations. Geoderma 37, 113–136.

Muller, J.-P., Calas, G., 1989. Tracing kaolinites through their defect centers; kaolinite paragenesis in a laterite (Cameroon). Econ. Geol. 84, 694–707.

Muller, J.P., Manceau, A., Calas, G., Th.; Ildefonse, P., Hazemann, J.L., 1995. Crystal chemistry of clays and associated oxides: constraints for modeling element transfer at the Earth's surface. Am. J. Sci. 295, 1115–1155.

Nahon, D., 1986. Evolution of iron crusts in tropical landscapes. In: Colman, S.M., Dethier, D.P. (Eds.), Rates of Chemical Weathering of Rocks and Minerals. Academic Press, Orlando, pp. 169–191.

Nahon, D., 1987. Microgeochemical environments in lateritic weathering. In: Rodriguez-Clemente, R., Tardy, Y. (Eds.), Geochemistry and Mineral Formation in the Earth Surface. pp. 141–156, Madrid.

Nahon, D., 1991. Self-organization in chemical lateritic weathering. Geoderma 51, 5–13.

Nahon, D., Janot, C., Karpoff, V., Paquet, H., Tardy, Y., 1977. Mineralogy, petrography and structures of iron crusts (ferricretes) developed on sandstones in the Western part of Senegal. Geoderma 19, 263–277.

Nishiizumi, K., Klein, J., Middleton, R., Craig, 1991a. Cosmic ray ^{10}Be and ^{26}AL in Antartic rocks: exposure and erosion history. Earth Planet. Sci. Lett. 104, 440–454.

Nishiizumi, K., Kohl, C.P., Shoemaker, E.M., Arnold, J.R., Klein, J., Fink, D., Middleton, R., 1991b. In situ ^{10}Be and ^{26}Al exposure ages at Meteor Crater, Arizona. Geochim. Cosmochim. Acta 55, 2699–2703.

Nishiizumi, K., Lal, D., Klein, J., Middleton, R., Arnold, J.R., 1986. Production of ^{10}Be and ^{26}Al by cosmic rays in terrestrial quartz in situ and implications for erosion rates. Nature 319, 134–136.

Nishiizumi, K., Winterer, E.L., Kohl, C., Klein, J., Middleton, R., Lal, D., Arnold, J.R., 1989. Cosmic ray production rates of ^{10}Be and ^{26}Al in quartz from glacially polished rocks. J. Geophys. Res. 94 (B12), 17907–17915.

O'Brien, K., 1979. Secular variations in the production of cosmo-

genic isotopes in the Earth's atmosphere. J. Geophys. Res. 84 (A2), 423–431.

Ojanuga, A.G., Lee, G.B., 1973. Characteristics, distribution, and genesis of nodules and concretions in soils of the South-Western Upland of Nigeria. Soil Sci. 116, 282–291.

Raisbeck, G.M., Yiou, F., 1980. ^{10}Be in polar ice as a record of solar activity. In: Pepin, R.O., Eddy, J.A., Merrill, R.B. (Eds.), Ancient Sun, pp. 185–190.

Raisbeck, G.M., Yiou, F., 1984. Production of long-lived cosmogenic nuclei and their applications. Nucl. Instrum. Methods Phys. Res., Sect. B B5, 91–99.

Raisbeck, G.M.; Yiou, F.; Bourlès, D.; Brown, E.; Deboffle, D.; Jouhanneau, P.; Lestringuez, J.; Zhou, Z.Q., 1994. The AMS facility at Gif-sur-Yvette: progress, perturbations and projects. Nucl. Instrum. Methods Phys. Res., Sect. B, B92, 43–46.

Raisbeck, G.M., Yiou, F., Bourlès, D.L., Lestringuez, J., Deboffle, D., 1987. Measurements of ^{10}Be and ^{26}Al with a Tandétron AMS facility. Nucl. Instrum. Methods Phys. Res., Sect. B 29, 22–26.

Robinson, C., Raisbeck, G.M., Yiou, F., Lehman, B., Laj, C., 1995. The relationship between ^{10}Be and geomagnetic field strength records in central North Atlantic sediments during the last 80 ka. Earth Planet. Sci. Lett. 136, 551–557.

Roche, E., 1987. Paléoenvironnement du Quaternaire supérieur au Shaba (Zaïre). Datation de deux "stone-lines" par palynologie: Kamoa et Haute Luilu. Geo-Eco-Trop 11 (1-4), 171–183.

Schwartz, D., 1996. Archéologie préhistorique et processus de formation des "stone-lines" en Afrique Centrale (Congo-Brazzaville et zones périphériques). Geo-Eco-Trop 20 (1-4), 15–38.

Segalen, P. 1994. Les sols ferralitiques et leur répartition géographique. Tome 1. Introduction générale. Les sols ferralitiques : leur identification et environnement immédiat. O.R.S.T.O.M. Paris, collect. Etudes et Thèses, 169 pp.

Sharma, P., Middleton, R., 1989. Radiogenic production of ^{10}Be and ^{26}Al in uranium and thorium ores: implications for studying terrestrial samples containing low levels of ^{10}Be and ^{26}Al. Geochim. Cosmochim. Acta 53, 709–716.

Stoops, G., 1967. Le profil d'altération du Bas-Congo (Kinshasa). Pedologie 17, 60–105.

Tardy, Y., 1993. Pétrologie des latérites et des sols tropicaux. Masson, Paris, 460 pp.

Tricart, J., 1976. Le modelé des régions chaudes. Traite Geomorphol.

Vogt, J., 1966. Terrains d'altération et de recouvrement en zone intertropicale. A-le complexe de la stone_line. Mise Point Bull. BRGM 4, 2–51.

Yiou, F., Raisbeck, G.M., Klein, J., Middleton, R., 1984. ^{26}Al/^{10}Be in terrestrial impact glasses. J. Non-Cryst. Solids 67 (1-3), 503–510.